Characterization of the Non-uniform Reaction in Chemically Amplified Calix[4]resorcinarene Molecular Resist Thin Films[1]

Vivek M. Prabhu,[A,F] *Shuhui Kang,*[A] *R. Joseph Kline,*[A]
Dean M. DeLongchamp,[A] *Daniel A. Fischer,*[B] *Wen-li Wu,*[A]
Sushil K. Satija,[C] *Peter V. Bonnesen,*[D] *Jing Sha,*[E] *and*
Christopher K. Ober[E]

[A]Polymers Division, National Institute of Standards and Technology, Gaithersburg,
MD 20899, USA.

[B]Ceramics Division, National Institute of Standards and Technology, Gaithersburg,
MD 20899, USA.

[C]Center for Neutron Research, National Institute of Standards and Technology,
Gaithersburg, MD 20899, USA.

[D]Center for Nanophase Materials Sciences, Oak Ridge National Laboratory, Oak Ridge,
TN 37831, USA.

[E]Cornell University, Materials Science and Engineering, Ithaca, NY 14853, USA.

[F]Corresponding author. Email: vprabhu@nist.gov

The *ccc* stereoisomer-purified *tert*-butoxycarbonyloxy-protected calix[4]resorcinarene molecular resists blended with photoacid generator exhibit a non-uniform photoacid-catalyzed reaction in thin films. The surface displays a reduced reaction extent, compared with the bulk, with average surface-layer thickness 7.0 ± 1.8 nm determined by neutron reflectivity with deuterium-labelled *tert*-butoxycarbonyloxy groups. Ambient impurities (amines and organic bases) are known to quench surface reactions and contribute, but grazing-incidence X-ray diffraction shows an additional effect that the protected molecular resists are preferentially oriented at the surface, whereas the bulk of the film displays diffuse scattering representative of amorphous packing. The surface deprotection reaction and presence of photoacid were quantified by near-edge X-ray absorption fine-structure measurements.

Introduction

Photoresist thin films are the enabling technology to fabricate nanoscale features for the semiconductor industry with photo-lithography.[1] However, imaging critical dimensions (CD) smaller than 22 nm with low line-edge roughness (LER) with 193-nm immersion and extreme-ultraviolet (EUV) lithography remains a challenge with chemically amplified resist materials that use blends of photoacid generator (PAG) with polymer. Alternative strategies with non-chemically amplified photo-resists are also considered for next-generation EUV lithography.[2,3] For chemically amplified resists, the quality of the patterned structures depends on sequential process steps that influence the spatial distribution of photoacids and the photo-acid-catalyzed reaction-diffusion process.[1,4–9] Controlling the reaction-diffusion process remains the predominant material strategy to achieve smaller CD and LER for the ultimate reso-lution of a printed feature.[10–14] However, because the photo-acid diffusion length (L_d) and the size of the resist polymer (R_g) have approached the length scales of the CD and LER,

alternative resists architectures are sought to maintain $L_d < CD$ and $R_g < CD$. The L_d may be reduced by increasing the molecular mass of the photoacid,[15–19] but this can lead to disadvantageous surface segregation and phase separation.[20,21] More recently, covalent bonding of the PAG to the polymer has shown markedly reduced L_d, as the acidic proton is restricted by the charge-neutralizing counter-ion covalently bound to the glassy polymer.[21–24] Alternatively, molecular resists are attractive owing to the smaller R_g, miscibility with photoacid generators[25] and well-defined molecular mass,[26] such that monodisperse distribution of protecting groups led to sub-30-nm features.[27] Measurements of the reaction-diffusion kinetics of molecular resists show that the deprotection reaction couples to the photoacid transport, hence L_d.[28,29] Measure-ments of the film reaction kinetics are necessary to develop predictable models to aid in resist design.[30–33]

Measurements that determine reaction kinetics with infrared spectroscopy average throughout the film thickness. Such approaches may not have the resolution or contrast to measure

---

[1]Official contribution of the National Institute of Standards and Technology; not subject to copyright in the United States

non-uniformities in sub-100-nm thin films. Deviations from bulk reactions at the interfaces become more important and can lead to surface (T-topping and closure) and substrate (undercutting and footing) defects on the final lithographic features.[34] Surface segregation of PAG was observed in polymer resists by near-edge X-ray absorption fine structure (NEXAFS) spectroscopy.[35–37] Time-of-flight secondary-ion mass spectrometry was used to show uniform depth profiles in optimized resist formulations under controlled-atmosphere clean-room conditions.[38] In addition to the non-uniform distribution of PAG, amine moieties in the ambient conditions quench the reaction at the free surface. Such effects are typically not considered by reaction kinetics studies because the film thickness to determine kinetics constants is usually larger, such that the surface does not contribute substantially to the change in bulk signal.

The reaction kinetics of chemically amplified molecular resists for next-generation lithography were previously quantified by time-resolved Fourier-transform infrared reflectance absorption spectroscopy.[28,29] This approach uses a bilayer film whereby a PAG is blended with resist and transferred on a PAG-free resist film on a silicon substrate[28,29] by the aid of a poly(dimethylsiloxane) (PDMS) stamp. This bilayer is then exposed to UV light and post-exposure baked (PEB) to provide a one-dimensional photoacid gradient that mimics a step-exposure line edge. Using the film-average composition change in films thicker than 100 nm, reaction kinetics constants and photoacid diffusion constants are estimated. However, on measuring the reaction front bilayers with high-resolution neutron reflectivity, the surface reaction was found to be inhibited, leaving a thin layer of highly protected resist that comprised less than 10 % of the 100-nm thin film (Accessory Publication, Fig. S1). The surface layer eventually completely deprotects with longer reaction time. Two experimental origins were suspected; the first was the use of the PDMS stamp, which may absorb and retain PAG, leaving the surface depleted of PAG. The second was the role of ambient amines that quench the photoacid at the surface to reduce the reactivity.[39,40]

Here, we demonstrate that this surface layer was not an artefact of the PDMS stamping, but a property of the purified *ccc* stereoisomer *tert*-butoxycarbonyloxy calix[4]resorcinarene (*t*-Boc-CM4R) molecular resist that preferentially orders at the free surface to kinetically limit the photoacid-catalyzed reaction. Neutron reflectivity provides a nanometre-resolution depth profile of the fraction of deprotection, whereas grazing-incidence X-ray diffraction (GIXD) quantifies the molecular order at the surface and bulk. The surface chemistry, characterized by NEXAFS, verifies the presence of photoacid as well as the change in surface reaction with reaction time and temperature within the top 1 to 6 nm. Although PAG segregation and surface-versus-bulk reactions are known in polymer resists,[35–37,41] such effects are less understood for well-defined molecular resists with low polydispersity.[42,43] Further, the alternative topology found with molecular resists may aid in the design of resists with order–disorder transitions. Such materials may find particular promise for thermal-induced scanning-probe lithography.[44]

Results and Discussion

Thin film blends of triphenylsulfonium perfluoro-butanesulfonate (TPS-PFBS) PAG and CM4R that was fully protected with deuterated *tert*-butoxycarbonyloxy groups (D-*t*-Boc-CM4R) were prepared as thin films on silicon wafer
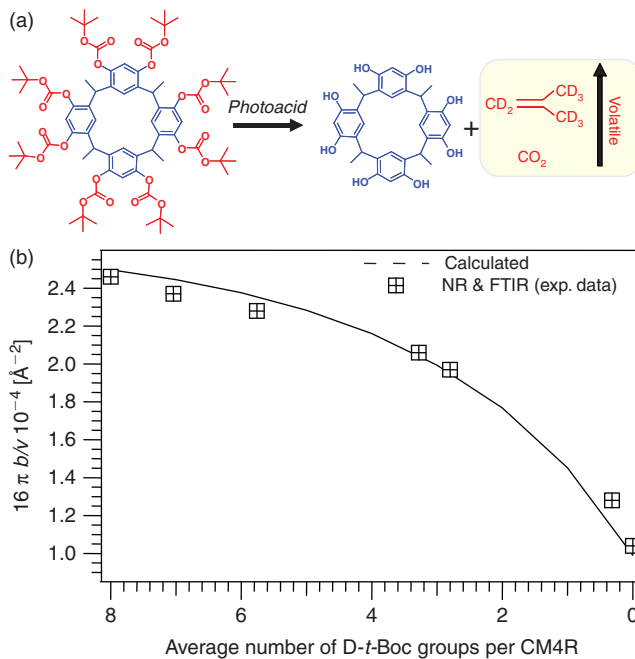
Fig. 1. (a) The photoacid-catalyzed deprotection of deuterated tert-butoxycarbonyloxy calix[4]resorcinarene (D-*t*-Boc-CM4R) is shown with main volatile products (carbon dioxide and deuteron-isobutene). The extent of reaction is dependent on reaction kinetics conditions. (b) Calculated and measured neutron scattering length density as a function of number of D-*t*-Boc groups per CM4R. Uncertainties are estimated to be less than 5 % based on propagation of angular and wavelength divergence used to fit the neutron scattering length density profiles within a given chi-squared statistic.

substrates. After a post-apply bake, the films were UV-exposed and PEB for 60 s at temperatures ranging from 60° to 80°C. This elevated temperature is required to increase the photoacid-catalyzed deprotection reaction rate of D-*t*-Boc-CM4R. On post-exposure baking, the D-*t*-Boc group leads to volatile deprotection products (carbon dioxide and deutero-isobutene) as shown in Fig. 1. The loss of deuterium protecting groups causes a decrease in film thickness proportional to the deprotection extent. The average film *t*-Boc protection level was characterized by infrared spectroscopy. The change in film D-*t*-Boc content also provides neutron reflectivity contrast, because deprotected CM4R and 100 % D-*t*-Boc-protected CM4R have a large scattering length density difference (Fig. 1). Neutron reflectivity methods can differentiate films that are deprotected uniformly from structures with buried interfaces.[45]

Fig. 2 shows neutron reflectivity data for five PEB temperatures as Fresnel-reduced reflectivity Q^4R versus Q, where R is the absolute reflectance and Q the wavevector. The reflectivity data (symbols) were fitted using the Parrat model (solid line) with the fit quality χ^2 statistic shown.[46] The interference of the reflected neutrons from the substrate and film interfaces leads to Kiessig fringes that are inversely proportional to the characteristic length (thickness) within the film plane. The total film thickness may be estimated directly from the fringe periodicity whereas fringe persistence provides evidence of the low surface roughness even after deprotection. The scattering length density (SLD = b/v) profiles that are results of the model slab fits are shown as $Q_c^2 = 16\pi b/v$ distance (Z) from the silicon substrate, silicon oxide, organic resist film, then air ($Q_c^2 = 0$). Where b is the total scattering length over all atomic elements per molecule within molecular volume v. This depth profiling in units of Q_c^2 shows that for each film, the surface maintains a higher SLD
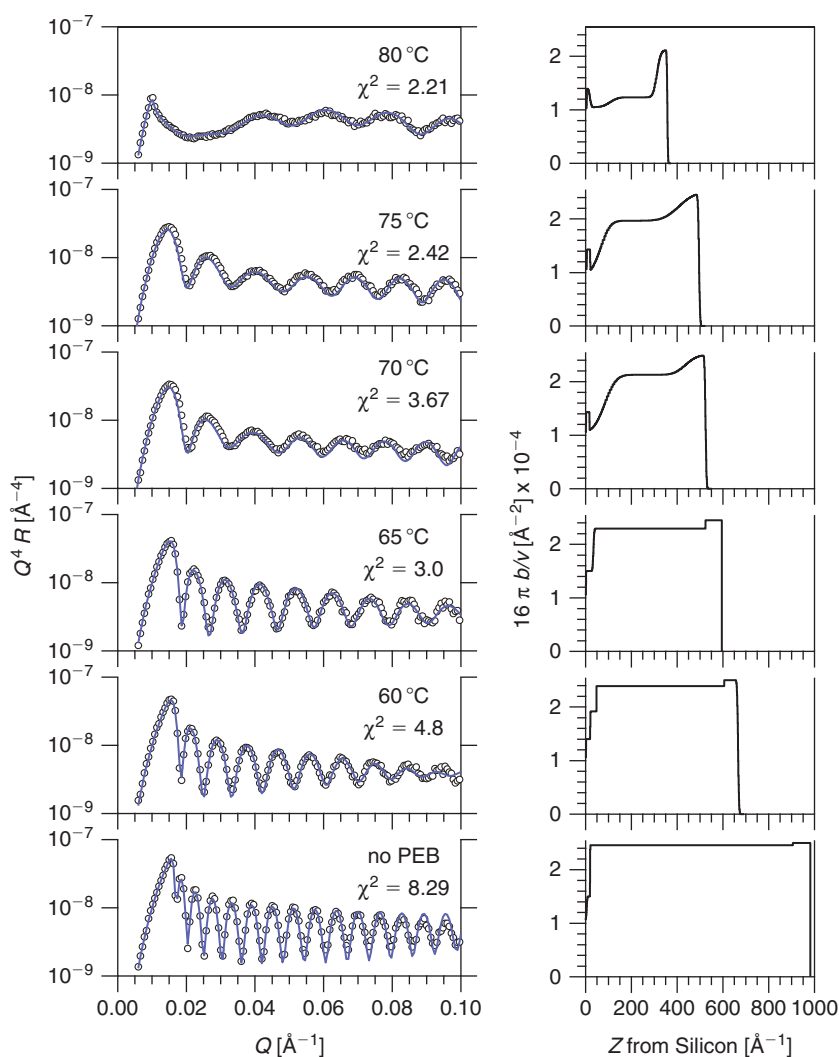
Fig. 2. (left panel) Fresnel-normalized neutron reflectivity as a function of post-exposure bake temperature after DUV exposure for single-layer films of D-*t*-Boc-CM4R blended with TPS-PFBS with Parratt model fits (solid lines); and (right panel) corresponding scattering length density profiles showing bulk reaction and surface-inhibited reaction extent.

than the bulk. The expected change in Q_c^2 for 100 % substituted to 0 % D-*t*-Boc-substituted CM4R was calculated as shown in Fig. 1. In Fig. 2, the surface remains highly protected, whereas the bulk of the film approaches the limiting value of 0 % protection ($Q_c^2 \approx 1 \times 10^{-4} \text{Å}^{-2}$) at the highest PEB temperature.

As the film reaction extent increases, the fraction of surface layer (slab thickness) to total film thickness increases with PEB temperature: 60°, 65°, 70°C, and 75° as 9, 12, 17 and 18 % respectively. Between 60° and 75°C after 60-s reaction time, the surface-layer Q_c^2 did not change, with average Q_c^2 (2.49 ± 0.025) × 10^{-4}Å^{-2} of thickness 7.5 ± 1.2 nm with uncertainties shown as one standard deviation. However, at 80°C, the surface-layer Q_c^2 reduced to $2.11 \times 10^{-4} \text{Å}^{-2}$ with thickness 4.5 nm, suggestive of significant deprotection and 13 % fraction of surface layer. The corresponding bulk of the film had Q_c^2 values of 2.39×10^{-4}, 2.3×10^{-4}, 2.1×10^{-4}, 1.97×10^{-4} and $1.23 \times 10^{-4} \text{Å}^{-2}$ for PEB temperatures 60°, 65°, 70°, 75° and 80°C respectively. Therefore, the bulk of the film proceeds with increasing reaction extent at higher temperatures. Fig. 1 shows the experimental average neutron Q_c^2 for the film versus the average degree of protection quantified by FT-IR. The agreement between the

experimental values and the calculated values based on mass density and chemical composition is excellent. Therefore, the surface maintains ~100 % D-*t*-Boc-CM4R (~$2.5 \times 10^{-4} \text{Å}^{-2}$) at lower reaction temperatures until the surface layer is deprotected to 45 % D-*t*-Boc-CM4R at 80°C. These data are only observations after fixed reaction times, but the observations of such a discrete layer at the surface with an interfacial width were unexpected.

The earliest analysis of *t*-Boc-protected polymer resists concluded that airborne contaminants quench the photoacid-catalyzed reaction at the near-surface, leading to T-topping and closure[39] defects. This was exacerbated by a prolonged post-exposure delay as found in poly(*t*-butoxycarbonyloxystyrene-sulfone)[47] and poly(4-*t*-butoxycarbonyloxystyrene) (PBOCSt)[39,48] resists that use the same protecting group as in this study and are also phenolic-based, as in CM4R. However, PAG surface segregation may also enhance the surface reaction, relative to the bulk, owing to higher concentration of photoacid at the surface in PBOCSt.[35] PAG segregation may be observed by X-ray reflectivity relying on the mass density contrast using iodonium-containing ionic PAGs at loadings up to 30 % by mass.[49] However, the neutron scattering
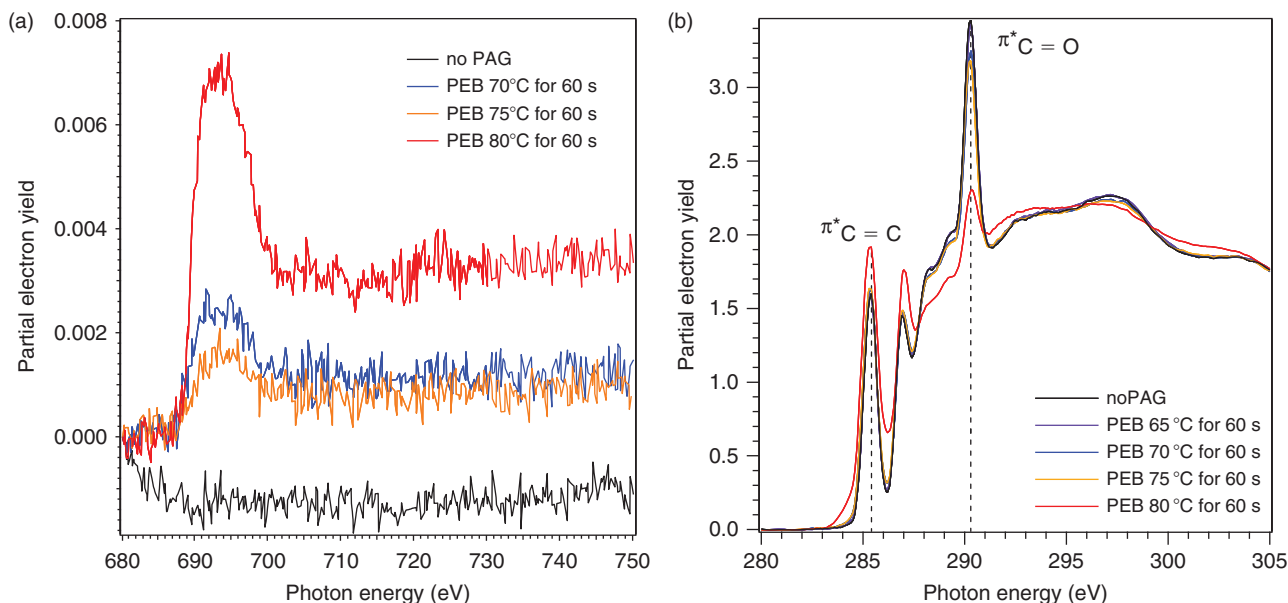
Fig. 3. Near-edge X-ray absorption fine structure (NEXAFS) (a) F *K*-edge showing presence of F–C bonds (~693 eV) content due to photoacid generator (PAG) with increase in relative concentration with post-exposure bake (PEB) temperature. (b) C *K*-edge showing loss of C=O (~290.3 eV) from *t*-Boc protecting groups with increasing PEB temperature and concurrent increase in C=C (~285 eV) due to increase in local concentration of aromatic species from calix[4]resorcinarene.

length density contrast between protected and partially deprotected D-*t*-Boc-CM4R makes the surface layer sensitive to the protection level rather than PAG. On UV exposure, the hydrogenous triphenyl groups of the PAG leave the film, with perfluorobutanesulfonic acid remaining. Characterization by NEXAFS at −150 V entrance-grid bias (EGB) on unexposed films shows that PAG is present at the surface in levels up to 10.6 % volume fraction via a linear least-squares fit of the C *K*-edge spectrum (Accessory Publication, Fig. S3), based on spectra normalized in the post-resonant region. The quality of fit is thus based on relative peak intensities and not the absolute intensity; the fit uncertainty is nevertheless extremely small because the spectral shapes of the components are quite different. This result proves that PAG is initially within the top 1 to 6 nm.

NEXAFS measurements at the fluorine *K*-edge show that photoacid is present at the surface after the post-exposure baking (Fig. 3a). The control film without any PAG of D-*t*-Boc-CM4R shows no F bonds. Therefore, the PAG-containing films, the same as those measured by neutron reflectivity, show F content (F–C bonds ≈ 693 eV) at the surface after UV exposure and post-exposure baking. The aromatic groups of the PAG leave the film after UV exposure with PFBS remaining in the film. As the post-exposure baking temperature increased, a relative increase in partial electron yield (PEY) was observed due to the increase in surface PFBS concentration caused by the volume loss by deprotection of D-*t*-Boc-CM4R. As the reaction occurs, the volatile D-*t*-Boc deprotection products increase the local PFBS concentration, as shown by the carbon *K*-edge data of Fig. 3b. The C *K*-edge shows a loss of $1s \rightarrow \pi^*_{C=O}$ (~290.3 eV) with increasing post-exposure baking temperature, with concurrent increase in C $1s \rightarrow \pi^*_{C=C}$ transition (~285 eV) due to an increase in concentration of aromatic species from CM4R. The largest decrease in C=O content occurs between 75° and 80°C, consistent with the observations of Fig. 2. The NEXAFS data shown in Fig. 3b are sensitive to the top 6 nm that includes the surface layer observed by neutron reflectivity. These NEXAFS data were used as independent data to refine the neutron

reflectivity model and served as a boundary condition to aid in the model fitting.

A difference between these D-*t*-Boc-CM4R materials and polymer resists is the ability for the 100 %-protected CM4R to crystallize because of the purification of the *ccc* stereoisomer form. On deprotection, a distribution of *ccc* and *ctt* stereoisomers may disrupt crystallization. GIXD provides surface sensitivity to the crystallinity and orientational order. When a highly collimated beam of X-rays are incident on a thin film below the film critical angle, an evanescent wave propagates along the film with depth that depends on the incidence angle α. Therefore, the near-surface structure may be measured with sensitivity distinct from the bulk depending on the grazing angle. The measurement of the diffracted intensity by an area detector provides reciprocal space information about the structure along the film thickness as well as the lateral order through intensity as a function of scattering vectors q_z and q_{xy}. The same thin films were examined by GIXD in Fig. 4 for the lowest (α = 0.06°, surfaces-sensitive) and largest (α = 0.12°, bulk-sensitive) grazing angle.

A control film with no PAG (no post-exposure bake) does not show any surface order, but a weak diffuse diffraction ring due to the amorphous packing of D-*t*-Boc-CM4R (Fig. 4) that is also prominent in the bulk scan. At 65°C, the bulk reaction occurs; however, GIXD only shows a weak diffuse ring and does not show surface structure. Only at temperatures greater than 65°C is the surface order observed, as seen by the weak diffraction arc in the 2D images along with the diffuse ring as summarized by the line-scan averages in Fig. 5. At 70° to 80°C, diffraction peaks appear as arcs centred at a well-defined q_z, as shown for the 75°C data. The fact that the diffraction in the surface-sensitive scans (α ≈ 0.06°) appears as arcs and not rings means the crystals near the surface are preferentially oriented. The diffraction peaks appear only along q_z and not as distinct spots within q_{xy}, consistent with a layered structure lacking in-plane order. Incident-angle-dependent NEXAFS spectra are unable to show significant molecular orientation at the surface (Accessory
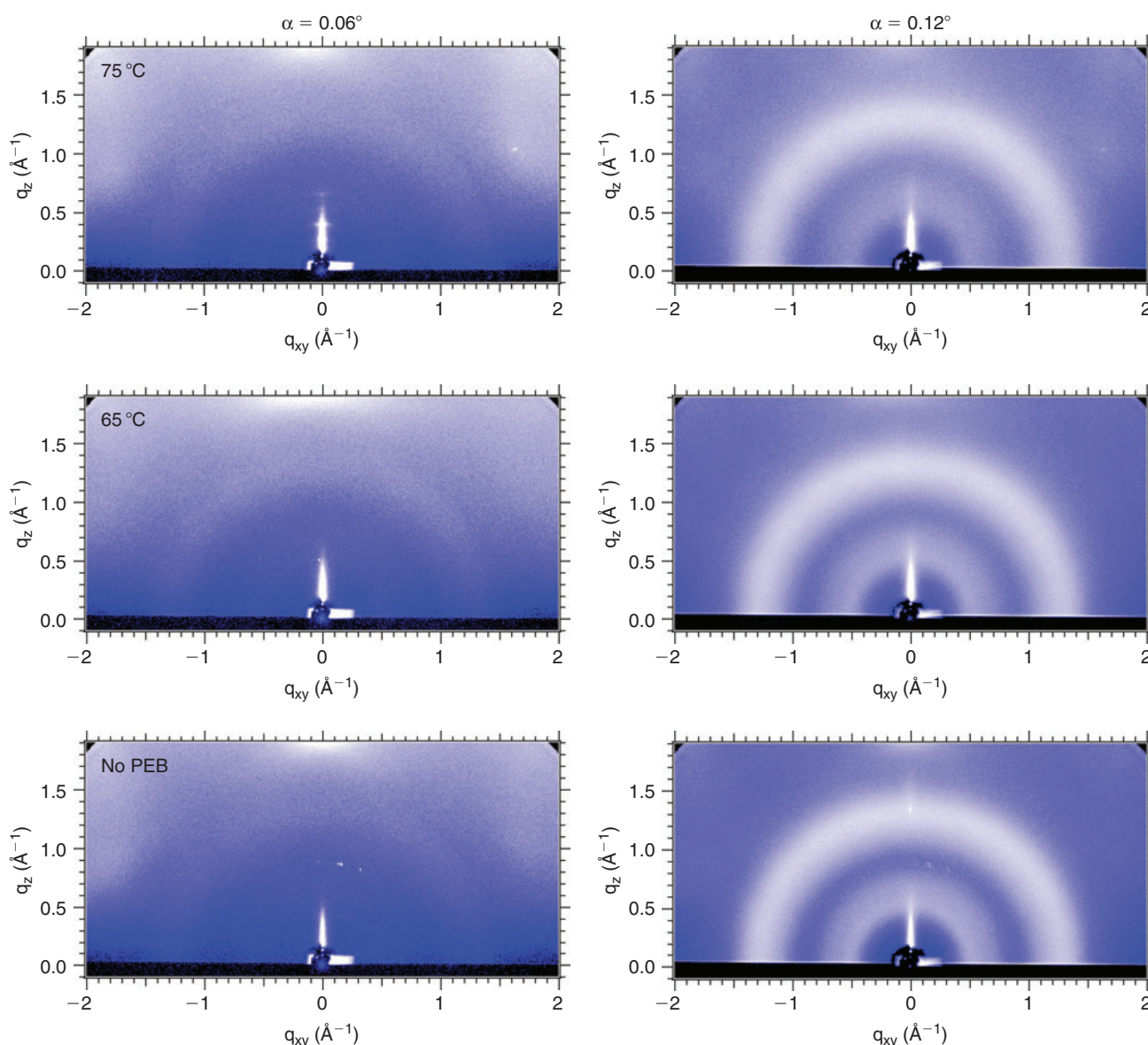
Fig. 4. Grazing-incidence X-ray diffraction for different post-exposure bake temperatures and a control film without photoacid generator and no post-exposure bake (PEB). Area detector shows sensitivity to the surface $\alpha \approx 0.06°$ and the bulk $\alpha \approx 0.12°$.

Publication, Fig. S4), owing to the lack of a common ring plane or linear backbone, which eliminates any significant aggregate transition dipole moment for the prominent resonances. The surface diffraction peak intensity increases with the post-exposure baking temperature (Fig. 5a), even though there is not substantial surface deprotection occurring at the surface below 80°C. The surface diffraction peaks are relatively sharp and have a vertical coherence length of 27, 20 and 37 nm for the 70°, 75° and 80°C post-exposure baking based on the Scherrer equation. This coherence length is larger than the surface-layer thickness measured in neutron reflectivity. It should be noted that the scattering intensity of the surface crystals is relatively weak and that concentrations of a few per cent would not affect the neutron reflectivity profiles. At lower reaction temperatures, the lack of surface order by GIXD may be due to too short reaction times. For instance, a longer reaction time, while leading to low deprotection extent, may provide sufficient kinetics of crystallization that become faster at higher temperatures.

At the highest grazing angle (0.12°), the X-rays penetrate through the entire film and represent a film-average structure as the signal from the surface is reduced. At all post-exposure baking temperatures, diffuse rings are observed indicative of amorphous films with substantially reduced diffraction from the crystals, consistent with a greater contribution of the bulk to the scattering signal. The low-q diffuse ring appears at $q^* \approx 0.54$ and 1.3 Å^{-1}, which correspond to characteristic lengths $(2\pi/q^*)$ of 1.16 and 0.48 nm respectively. As the bulk reaction occurs, the low-q amorphous ring disappears, suggesting that this characteristic length is associated with the D-t-Boc-protected upper rim of CM4R, as at 80°C, the reaction is near complete within the bulk, whereas the high-q peak broadens with peak position relatively unchanged, suggestive of structural origin within the aromatic crown of the CM4R with little dependence on degree of D-t-Boc substitution. The decrease in intensity could be due to the loss in contrast via loss in O content from the volatile protecting group products (CO_2). The mean distance between methyl-substituted bridging carbons was ~0.51 nm,[50]
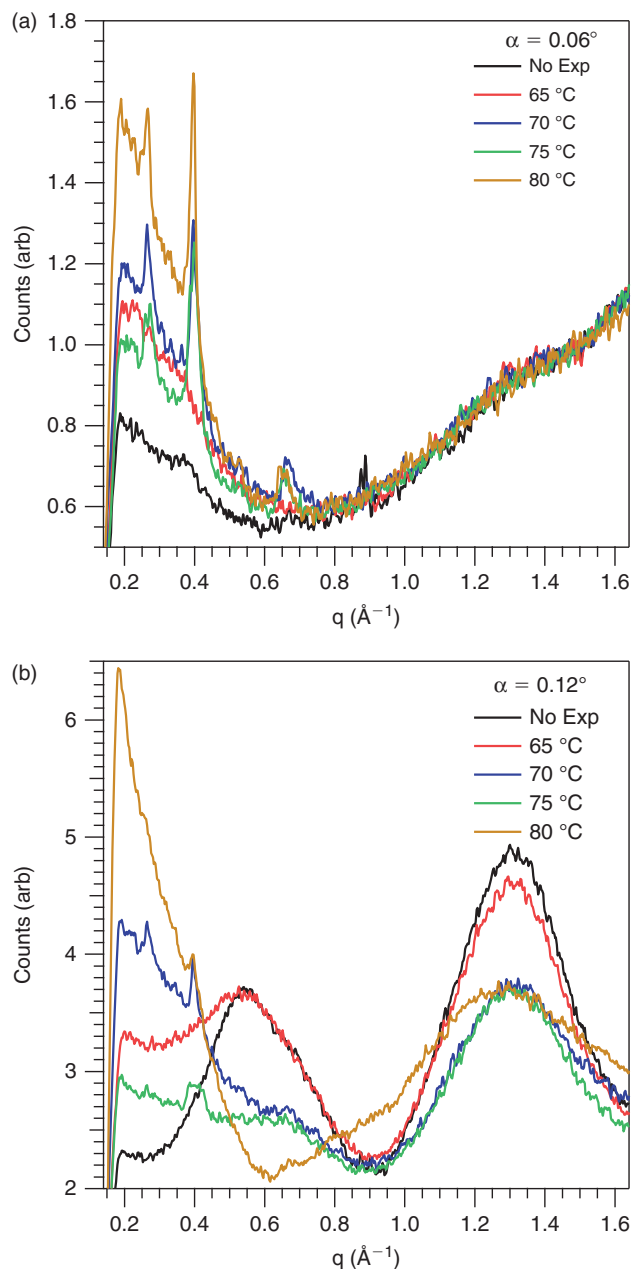
Fig. 5. Grazing incidence X-ray diffraction (GIXD) line scan averages along q_z cut for the (a) surface, and (b) bulk incidence angles. Note that in the GIXD geometry, the specular conditions are not met and the axis labeled q_z is several degrees away from the sample normal dependent on the q.

Fig. 6. Composite hypothesis using the neutron reflectivity depth profile plotted as average number of D-*t*-Boc-substituted CM4R (degree of protection) for two different post-exposure bake (PEB) temperatures.

as found in CM4R co-crystals. It is hypothesized that the presence of the surface order may exclude photoacid generator, such that deprotection is kinetically limited by the less accessible *t*-Boc groups within the ordered domains and reduced average diffusivity of photoacid that remains blended with amorphous D-*t*-Boc-CM4R material at the surface. On average, the kinetics of deprotection are suppressed by the presence of the ordered and oriented D-*t*-Boc-CM4R.

The depth profiles of neutron reflectivity combined with the GIXD data allow us to develop a refined hypothesis for the lack of surface deprotection in these purified D-*t*-Boc-CM4R resist PAG blends. Fig. 6 shows a composite plot for the film thickness dependence on average D-*t*-Boc protection level. The solid lines show the surface, bulk and substrate

dependence of the D-*t*-Boc protection. The surface of the films forms a layer that contains a mixture of preferentially ordered and oriented D-*t*-Boc-CM4R, but in the presence of photoacid and amorphous D-*t*-Boc-CM4R, as shown by NEXAFS. Between 75° and 80°C, bulk deprotection occurs, enabled by dispersed photoacid, as well as surface deprotection such that the average surface deprotection level decreases, but maintains a fraction of the surface ordered 100 % D-*t*-Boc-CM4R. At this point, we cannot quantify the degree of crystallinity at the surface, but these data are the first to show that the surface order persists as a discrete layer.

The structure of the ordered phase appears to have order primarily along the film thickness (q_z). The molecular crystal structure is not known for these materials and comparison with the unprotected CM4R may be erroneous because the protection groups could change the unit cell dimensions that contain a different number of D-*t*-Boc-CM4R and possibly be co-crystallized with solvent. The data do imply a first-order (hidden by the beam stop) d-spacing of 4.7 nm owing to the observed second, third (highest-intensity) and fifth order peaks. The non-monotonic decay of intensity versus peak order is consistent with a complex structure in the unit cell, which would be consistent with multiple molecules per unit cell. A higher-order structure such as a lamellar phase cannot be ruled out, if the repeat is larger than that of the molecular unit-cell dimension, considering the one-dimensional order with lack of in-plane structure. However, the persistence of the diffraction at the surface with reduced presence in the bulk along with the

estimate of the crystal size are suggestive of a population of crystals that extend from the surface layer into the bulk of the film. The relatively large crystals could contribute to the observed interfacial width between the bulk of the film and surface layer via a heterogeneous interface of extended crystals of varying length within a deprotected matrix, rather than a smooth compositional gradient of protection level. Off-specular reflectivity could probe such a buried interface.

Experimental

Materials and Film Processing

tert-Butoxycarbonyloxy-protected calix[4]resorcinarene molecular resists were synthesized with deuterium-substituted *tert*-butoxycarbonyl (D-*t*-Boc) protecting groups (Fig. 1) on each of the eight CM4R hydroxyl moieties. The PAG used was TPS-PFBS (Sigma–Aldrich). Solutions of D-*t*-Boc-CM4R/ TPS-PFBS were prepared for spin-coating with 5 % PAG by mass of solids in toluene at a concentration of 2 % by mass. This solution was spin-coated onto clean silicon wafers (76 mm diameter, 800 μm thick, Virginia Semiconductor Inc.) followed by a post-apply bake (PAB) for 60 s at 80°C with a Brewer Science CEE hotplate with vacuum contact. The initial film layer thickness before reaction was ∼100 nm. Subsequently, a dose of ∼150 mJ cm^{-2} from an Oriel UV exposure system with 248-nm broadband radiation activated all the PAG. Post-exposure bake was performed at temperatures from 60° to 80°C for 60 s. After the post-exposure bake, a noticeable film thickness change was observed by the change in colour of the reflected ambient light. The average deprotection level of D-*t*-Boc-CM4R was quantified by the loss in C=O stretch ($v_{C=O} \approx 1760\,cm^{-1}$) by FT-IR using a Bomem FTLA 2000 instrument in reflection mode at 16-cm^{-1} resolution as described in detail elsewhere.[28]

Neutron Reflectivity

Specular neutron reflectivity was performed on the NG7 horizontal cold neutron reflectometer at the NIST Center for Neutron Research. The reflectivity was normalized by the incident beam intensity and measured as a function of the wave vector (Q) normal to the film, $Q = 4\pi/\lambda \sin\theta$, where λ is the incident neutron wavelength of 4.75 Å and θ is the specular angle of reflection. The specular reflected intensity provides a nanometre-resolution depth profile of the film due to neutron scattering length density variations (contrast). The scattering length density (SLD = b/v) is quantified by the total scattering length ($b = \sum b_i$ over all atomic elements per molecule) within molecular volume v and often reported as $Q_c^2 = 16\pi b/v$. Although the atomic scattering length (b_i) varies from element to element, a large scattering-length difference occurs between hydrogen ($b_H = -0.374 \times 10^{-12}\,cm$) and deuterium ($b_D = 0.667 \times 10^{-12}\,cm$) isotopes. Therefore, the contrast in a neutron reflectivity experiment may be enhanced by deuterium substitution to measure composition profiles with nanometre resolution. The reflectivity data were fitted to the results calculated from the modelled depth profiles using the Parratt algorithm in units of SLD using the NIST *Reflpak* software.[46] In general, this approach uses successive slab layers of constant SLD with interfaces smeared by a Gaussian function. By varying the slab fit parameters (SLD, absorption, thickness and roughness), a multilayered model can be established to determine the best fit with the χ^2 statistic. The SLD may be calculated knowing the chemical composition and mass density. Calculations for the SLD versus number of *t*-Boc per CM4R are shown

as the dashed lines in Fig. 1 for per-deuterated *t*-Boc-protected CM4R. The mass density was determined by X-ray reflectivity on pure-component thin film control samples without PAG. The box symbols are the experimentally determined average SLD for partially reacted thin films with an average deprotection extent determined by infrared spectroscopy. The experiment and model agreement allows a mapping of SLD to average fraction of D-*t*-Boc-CM4R protection level. Uncertainties are calculated as the estimated standard deviation from the mean. In the case where the limits are smaller than the plotted symbols, the limits are removed for clarity. Estimation of the total error in the extracted fit parameters (SLD and film profiles) is difficult as the precision of the fit parameters, determined by the inverse of the curvature matrix is, in general, less than the significant figures reported.[51]

Near-edge X-ray Absorption Fine Structure Spectroscopy

Near edge X-ray absorption fine structure spectroscopy measurements were conducted at the NIST/Dow soft X-ray material characterization facility, beamline U7A of the National Synchrotron Light Source at Brookhaven National Laboratory. In a NEXAFS experiment, tunable soft X-rays are preferentially absorbed by the sample (characteristic depth of ∼200 nm) when the incident radiation is at the appropriate energy to allow the excitation of a core-shell electron of a specific element (C, N, O or F) to a chemical bond-specific unoccupied molecular orbital.[52] Owing to the well-defined energy gap associated with a core shell to unoccupied orbital transition, NEXAFS is sensitive to the bonding characteristics of the element, giving a discrete peak for each chemical bond. Auger electrons and fluorescence photons are emitted when the excited core hole from the irradiated sample relaxes. Auger electrons emitted from deep (>10 nm) within the film undergo multiple inelastic scattering and lose their kinetic energy within the film and hence cannot escape the surface potential to reach the detector. In contrast, electrons originating from near the top (1 to 6 nm for carbon *K*-edge electron yield spectra) of the film surface have sufficient kinetic energy to escape the surface potential. Electrons that escape the surface potential will have different final kinetic energies on detection depending on their inelastic energy loss (depth of creation). By applying a negative voltage EGB at the PEY detector, electrons of low kinetic energy can be rejected. As the negative EGB is gradually increased, lower-kinetic-energy electrons are discriminated against and the effective electron yield sampling depth gets closer to the film surface. This scheme uses EGB from −50 to −250 V, probing the top 6 to 1 nm respectively. The spectra were collected with the incident beam (I_o) at the magic angle (54.7°) relative to the sample to remove any polarization dependence of the NEXAFS intensities. All PEY spectra in this paper were I_o-normalized for beam instabilities and monochromator abortion features using the total yield of clean gold I_o mesh placed in the incident beam before the sample. Carbon *K*-edge spectra were collected in PEY mode with a grid bias of −50 V. Spectra fitted to a composition ratio were pre-edge normalized via subtraction to make the average intensity in the range of 280 to 283 eV zero. The standard uncertainty in PEY is ±2 % and photon energy is ±0.2 eV.

Grazing-incidence X-ray Diffraction

Grazing incidence X-ray diffraction was performed on beam line 11–3 at Stanford Synchrotron Radiation Lightsource (SSRL) with photon energy of 12.73 keV. The diffraction patterns were recorded using a two-dimensional plate detector (MAR-345) with a spatial resolution of 150 μm (2300 × 2300)

pixels that was located at a distance of 400.8 mm from the sample centre. The incidence angle was optimized such that signal-to-background ratio was maximized and typically, the angle between the incident beam and the sample surface was varied between 0.06°, 0.08°, 0.10° and 0.12° to provide depth sensitivity. The surface sensitivity is highest at 0.06°.

Conclusions

Advances to novel photosensitive-materials architectures are required to extend photolithography to feature sizes below 22 nm. Molecular resists offer one possibility by reducing the resist size while maintaining processability. Model purified *ccc* stereoisomer D-*t*-Boc-CM4R exhibits thin film structure not observed by polymer resists. A reduced surface extent of reaction appears in spin-cast PAG-containing films not caused by PAG depletion. The reduced reaction extent was aided by an ordered surface phase. It is not understood what determines the length scale of the surface layer of between 4 to 7 nm, rather than the entire film. However, it is a kinetic transient that appears for short reaction times. Further, the role of spin-coating solvent and plasticization by volatile reaction products at elevated temperatures cannot be ruled out, as the degree of surface-order diffraction intensity increased with average reaction extent. Although typical photoresist formulations do not contain such highly purified isomers, these monodisperse materials are model systems, especially as polydispersity was shown to affect patternability[42,43] and is a design criterion. The applications of pure stereoisomer CM4R are also important as additives to polymer resists formulations.[53] Therefore, the structure of blends of polymer and molecular resists may offer important practical remedies in photolithography.

Accessory Publication

Accessory neutron reflectivity and near-edge X-ray absorption fine structure data on bilayers and single layer films for this article are available on the Journal's website.

Acknowledgements

References

[1] H. Ito, *Adv. Polym. Sci.* **2005**, *172*, 37.

[2] A. G. Yu, H. P. Liu, J. P. Blinco, K. S. Jack, M. Leeson, T. R. Younkin, A. K. Whittaker, I. Blakey, *Macromol. Rapid Commun.* **2010**, *31*, 1449. doi:10.1002/MARC.201000117

[3] K. J. Lawrie, I. Blakey, J. P. Blinco, H. H. Cheng, R. Gronheid, K. S. Jack, I. Pollentier, M. J. Leeson, T. R. Younkin, A. K. Whittaker, *J. Mater. Chem.* **2011**, *21*, 5629. doi:10.1039/C0JM03288C

[4] W. Hinsberg, F. A. Houle, J. Hoffnagle, M. Sanchez, G. Wallraff, M. Morrison, S. Frank, *J. Vac. Sci. Technol. B* **1998**, *16*, 3689. doi:10.1116/1.590392

[5] A. Pawloski, A. Acheta, I. Lalovic, B. LaFontaine, H. Levinson, *Proceedings of the SPIE, Advances in Resist Technology and Processing XXI* **2004**, *5376*, 414.

[6] H. Ito, *J. Polym. Sci. A Polym. Chem.* **2003**, *41*, 3863. doi:10.1002/POLA.10963

[7] C. Willson, H. Ito, J. Frechet, T. Tessier, F. Houliham, *J. Electrochem. Soc.* **1986**, *133*, 181. doi:10.1149/1.2108519

[8] F. A. Houle, W. D. Hinsberg, M. I. Sanchez, J. A. Hoffnagle, *J. Vac. Sci. Technol. B* **2002**, *20*, 924. doi:10.1116/1.1475985

[9] G. M. Wallraff, W. D. Hinsberg, *Chem. Rev.* **1999**, *99*, 1801. doi:10.1021/CR980003I

[10] J. H. Kim, Y. H. Kim, S. M. Chon, T. Nagai, M. Noda, Y. Yamaguchi, Y. Makita, H. Nemoto, *J. Photopolym. Sci. Technol.* **2004**, *17*, 379. doi:10.2494/PHOTOPOLYMER.17.379

[11] G. M. Schmid, M. D. Stewart, V. K. Singh, C. G. Willson, *J. Vac. Sci. Technol. B* **2002**, *20*, 185. doi:10.1116/1.1431954

[12] M. D. Stewart, H. V. Tran, G. M. Schmid, T. B. Stachowiak, D. J. Becker, C. G. Willson, *J. Vac. Sci. Technol. B* **2002**, *20*, 2946. doi:10.1116/1.1523027

[13] J. A. Hoffnagle, W. D. Hinsberg, M. I. Sanchez, F. A. Houle, *Opt. Lett.* **2002**, *27*, 1776. doi:10.1364/OL.27.001776

[14] *International Technology Roadmap for Semiconductors 2009 Edition* 2009, Lithography Section, p. 9. Available at: http://www.itrs.net, verified July 2011.

[15] T. Itani, H. Yoshino, M. Fujimoto, K. Kasama, *J. Vac. Sci. Technol. B* **1995**, *13*, 3026. doi:10.1116/1.588315

[16] W. D. Hinsberg, F. A. Houle, M. Sanchez, M. Morrison, G. M. Wallraff, C. Larson, J. Hoffnagle, P. Brock, G. Breyta, *Proceedings of the SPIE, Advances in Resist Technology and Processing XVII* **2000**, *3999*, 148.

[17] S. L. Ablaza, J. F. Cameron, G. Y. Xu, W. Yueh, *J. Vac. Sci. Technol. B* **2000**, *18*, 2543. doi:10.1116/1.1288136

[18] H. Iwasaki, T. Itani, M. Fujimoto, K. Kasama, *Proc. of SPIE* **1994**, *2195*, 164.

[19] B. D. Vogt, S. Kang, V. M. Prabhu, E. K. Lin, S. K. Satija, K. Turnquest, W. Wu, *Macromol* **2006**, *39*, 8311. doi:10.1021/MA061209L

[20] N. Sundararajan, C. Keimel, N. Bhargava, C. Ober, J. Opitz, R. D. Allen, G. Barclay, G. Xu, *J. Photopolym. Sci. Technol.* **1999**, *12*, 457. doi:10.2494/PHOTOPOLYMER.12.457

[21] T. H. Fedynyshyn, D. K. Astolfi, A. Cabral, J. Roberts, *Proc. SPIE* **2007**, *6519*, X5190.

[22] Y. Fukushima, T. Watanabe, R. Ohnishi, H. Kinoshita, H. Shiotani, S. Suzuki, M. Hayakawa, Y. Endo, T. Yamanaka, S. Yusaa, *J. Photopolym. Sci. Technol.* **2007**, *20*, 419. doi:10.2494/PHOTOPOLYMER.20.419

[23] R. D. Allen, P. J. Brock, Y. H. Na, M. H. Sherwood, H. D. Truong, G. M. Wallraff, M. Fujiwara, K. Maeda, *J. Photopolym. Sci. Technol.* **2009**, *22*, 25. doi:10.2494/PHOTOPOLYMER.22.25

[24] R. Gronheid, A. V. Pret, B. Rathsack, J. Hooge, S. Scheer, K. Nafus, H. Shite, J. Kitano, *Journal of Micro-Nanolithography, MEMS and MOEMS* **2011**, *10*, 013017.

[25] D. L. VanderHart, V. M. Prabhu, A. De Silva, N. M. Felix, C. K. Ober, *J. Mater. Chem.* **2009**, *19*, 2683. doi:10.1039/B816290E

[26] H. Oizumi, Y. Tanaka, T. Kumise, D. Shiono, T. Hirayama, H. Hada, J. Onodera, A. Yamaguchi, I. Nishiyama, *J. Photopolym. Sci. Technol.* **2007**, *20*, 403. doi:10.2494/PHOTOPOLYMER.20.403

[27] T. Owada, H. Shiotani, K. Aoyama, T. Kashiwamura, M. Shibata, T. Takeya, H. Oizumi, T. Itani, *Proc. SPIE* **2010**, *7636*, 32. doi:10.1117/12.846069

[28] S. H. Kang, W. L. Wu, K. W. Choi, A. De Silva, C. K. Ober, V. M. Prabhu, *Macromol* **2010**, *43*, 4275. doi:10.1021/MA902548A

[29] J. Sha, J. K. Lee, S. H. Kang, V. M. Prabhu, C. L. Soles, P. V. Bonnesen, C. K. Ober, *Chem. Mater.* **2010**, *22*, 3093. doi:10.1021/CM9038939

[30] F. A. Houle, W. D. Hinsberg, M. Morrison, M. I. Sanchez, G. Wallraff, C. Larson, J. Hoffnagle, *J. Vac. Sci. Technol. B* **2000**, *18*, 1874. doi:10.1116/1.1303753

[31] B. Rathsack, K. Nafus, S. Hatakeyama, Y. Kuwahara, J. Kitano, R. Gronheid, A. V. Pret, *Proc. SPIE* **2009**, *7273*, 47. doi:10.1117/12.814287

[32] M. D. Smith, C. A. Mack, *Proc. SPIE* **2003**, *5040*, 1509. doi:10.1117/12.485541

[33] M. D. Smith, J. D. Byers, C. A. Mack, *Proc. SPIE* **2004**, *5376*, 322. doi:10.1117/12.537581

[34] R. Gronheid, B. Rathsack, S. Bernard, A. V. Pret, K. Nafus, S. Hatakeyama, *J. Photopolym. Sci. Technol.* **2009**, *22*, 97. doi:10.2494/PHOTOPOLYMER.22.97

[35] J. L. Lenhart, R. L. Jones, E. K. Lin, C. L. Soles, W. L. Wu, D. A. Fischer, S. Sambasivan, D. L. Goldfarb, M. Angelopoulos, *J. Vac. Sci. Technol. B* **2002**, *20*, 2920. doi:10.1116/1.1524970

[36] J. L. Lenhart, D. A. Fischer, S. Sambasivan, E. K. Lin, R. L. Jones, C. L. Soles, W. L. Wu, D. L. Goldfarb, M. Angelopoulos, *Langmuir* **2005**, *21*, 4007. doi:10.1021/LA047160Z

[37] V. M. Prabhu, S. Sambasivan, D. Fischer, L. K. Sundberg, R. D. Allen, *Appl. Surf. Sci.* **2006**, *253*, 1010. doi:10.1016/J.APSUSC.2006.03.089

[38] T. Hirayama, D. Shiono, J. Onodera, A. Yamaguchi, H. Fukuda, *Polym. Adv. Technol.* **2006**, *17*, 116. doi:10.1002/PAT.670

[39] W. D. Hinsberg, S. A. Macdonald, N. J. Clecak, C. D. Snyder, *Chem. Mater.* **1994**, *6*, 481. doi:10.1021/CM00040A024

[40] F. A. Houle, W. D. Hinsberg, M. I. Sanchez, *J. Vac. Sci. Technol. B* **2004**, *22*, 747. doi:10.1116/1.1688351

[41] E. L. Jablonski, V. M. Prabhu, S. Sambasivan, D. A. Fischer, E. K. Lin, D. L. Goldfarb, M. Angelopoulos, H. Ito, *Proceedings of the SPIE, Advances in Resist Technology and Processing XXI* **2004**, *5376*, 302–11.

[42] D. Shiono, H. Hada, H. Yukawa, H. Oizumi, L. Nishiyama, K. Kojima, H. Fukuda, *Advances in Resist Materials and Processing Technology XXIV* **2007**, *6519*, U5193.

[43] D. Shiono, H. Hada, H. Yukawa, H. Oizumi, I. Nishiyama, K. Kojima, H. Fukuda, *Microelectron. Eng.* **2007**, *84*, 1084. doi:10.1016/J.MEE.2007.01.146

[44] D. Pires, J. L. Hedrick, A. De Silva, J. Frommer, B. Gotsmann, H. Wolf, M. Despont, U. Duerig, A. W. Knoll, *Science* **2010**, *328*, 732. doi:10.1126/SCIENCE.1187851

[45] V. M. Prabhu, S. H. Kang, D. L. VanderHart, S. K. Satija, E. K. Lin, W. L. Wu, *Adv. Mater.* **2011**, *23*, 388. doi:10.1002/ADMA.201001762

[46] P. A. Kienzle, K. V. O'Donovan, J. F. Ankner, N. F. Berk, C. F. Majkrzak, *NCNR Reflectometry Software* **2006** Available at: http://www.ncnr.nist.gov/reflpak, verified July 2011.

[47] O. Nalamasu, E. Reichmanis, J. E. Hanson, R. S. Kanga, L. A. Heimbrook, A. B. Emerson, F. A. Baiocchi, S. Vaidya, *Polym. Eng. Sci.* **1992**, *32*, 1565. doi:10.1002/PEN.760322104

[48] S. A. MacDonald, W. D. Hinsberg, H. R. Wendt, N. J. Clecak, C. G. Willson, C. D. Snyder, *Chem. Mater.* **1993**, *5*, 348. doi:10.1021/CM00027A018

[49] T. Fukuyama, T. Kozawa, S. Tagawa, R. Takasu, H. Yukawa, M. Sato, J. Onodera, I. Hirosawa, T. Koganesawa, K. Horie, *Applied Physics Express* **2008**, *1*, 065004.

[50] R. Kuzmicz, V. Kowalska, S. Domagala, M. Stachowicz, K. Wozniak, W. Kolodziejski, *J. Phys. Chem. B* **2010**, *114*, 10311. doi:10.1021/JP1015565

[51] P. R. Bevington, *Data Reduction and Error Analysis for the Physical Sciences* **1969** (McGraw-Hill: New York).

[52] J. Stöhr, *NEXAFS Spectroscopy* **1992** (Springer-Verlag: New York).

[53] H. Ito, T. Nakayama, M. Sherwood, D. Miller, M. Ueda, *Chem. Mater.* **2008**, *20*, 341. doi:10.1021/CM7021483